On the Design of Pattern Reconfigurable Alford Loop Antennas

Md Abu Saleh Tajin and Kapil R. Dandekar Electrical and Computer Engineering Drexel University, Philadelphia, PA 19104, USA Email: {mt3223, dandekar}@drexel.edu

Abstract—We present a step-by-step approach for designing a recofigurable Alford loop antenna (RALA). The design of an 3.5 GHz RALA is shown. The antenna is fabricated using a 1.6 mm thick double-sided FR4 substrate. We sweep antenna geometrical parameters and show the effect on antenna input impedance, reflection coefficient (S_{11}) , and radiation patterns. The final antenna structure resonates at 3.5 GHz with eight directional and one omnidirectional radiation patterns. We also present a simplistic control circuit responsible for activating the antenna elements. Tri-state impedance matching- a major challenge in the design of RALA is also discussed and analyzed along with a proposed method for mitigation. 3D radiation patterns of the RALA was measured using an EMScan and a maximum gain of 4.5 dBi is found.

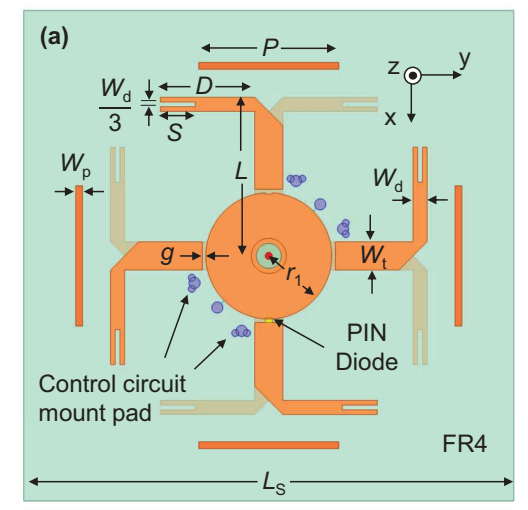
 ${\it Index\ Terms} {\color{red}\textbf{--}} Reconfigurable\ Alford\ loop\ antenna\ (RALA), reconfigurable\ antenna$

I. INTRODUCTION AND RELATED WORK

Reconfigurable antennas have drawn significant attention from the research community due to their dynamic nature that allows for efficient and adaptive utilization of wireless communication channels [1]. A reconfigurable antenna is capable of changing its operating frequency, bandwidth, radiation pattern, or polarization in response to the needs of the overlying communication system [2].

A RALA, with pattern reconfigurability features, is a two-layer printed circuit board (PCB) antenna capable of generating directional and omnidirectional radiation beams based on direct current (DC) control inputs. The antenna has four directional dipole elements (Fig. 1). Each antenna element can be separately or simultaneously activated to generate directional or omnidirectional radiation patterns. The control circuit for each element, consisting of a PIN diode [3], light emitting diode (LED), resistor, and inductor (choke), is activated by a 3V DC supply. The RALA can generate eight directional beams (45° angular separation) and one omnidirectional beam. RALA antennas were primarily developed for wireless local area network (WLAN) applications. Reconfigurable Alford loops have been used for mitigating interference in a multiuser MIMO system [4].

Patron *et al.* proposed reconfigurable Alford loop antennas (RALAs) at 3.8 GHz [5–7] and 2.6 GHz [8]. The antenna elements can be activated by external DC control signals. In addition, optical control of RALA elements has also been presented [9]. The performance of RALA has been evaluated



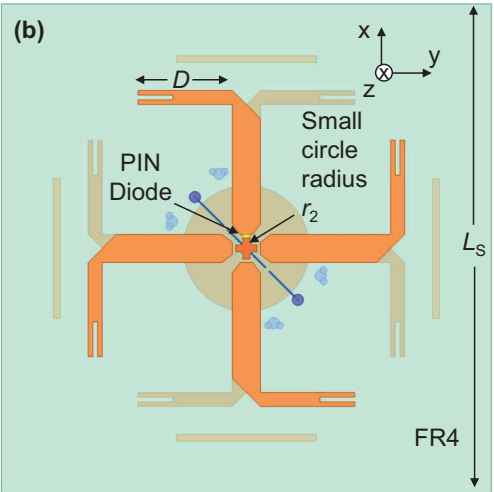


Fig. 1: (a) Top and (b) bottom layers of the 3.5 GHz RALA. The thickness of the FR4 substrate is 1.6 mm.

for multiple-input multiple-output (MIMO) systems [10]. A dual-band (2.4 GHz and 5 GHz) RALA has also been proposed using lumped filters [11]. Gao *et al.* developed a reconfigurable antenna [12] that is beam-steerable and frequency-reconfigurable, offering attractive features. However, multi-

TABLE I: 3.5 GHz RALA Initial Design Parameters

Parameter	Value (mm)	Parameter	Value (mm)
D	13.5	L	22.6
$L_{\rm S}$	70	P	20
r_1	9	r_2	1
$W_{\rm p}$	1	W_{d}	2
S	5	g	0.5

feature reconfigurability comes at the price of increased complexity in antenna geometry and fabrication.

Efficient implementation of the RALA requires automated selection of optimum beams based on the need of the overlying wireless network. Machine learning-based beam selection techniques [13,14] for RALAs have been proposed and experimentally validated. The antenna is capable of selecting an optimum beam based on the channel state information (CSI).

In this work, we present a generalized strategy for designing RALAs. The steps for designing a 3.5 GHz RALA relevant for 5G New Radio (5G NR) are shown. Moreover, the associated challenges and directionality-matching trade-offs are also discussed. We also show a simpler control circuit for the RALA, without using field effect transistors (FETs).

The operational modes of the RALA can be divided into three categories- *i*) single mode: only one element is activated at a time, *ii*) dual mode: two consecutive elements are activated simultaneously, and *iii*) omni mode: all four elements are activated at the same time. The input impedance values of the antenna are different for the three modes. As a result, it is challenging to match the antenna in all three modes. In this work, we show that if the antenna is impedance-matched in the single mode, the dual and omni mode impedance values are increasingly harder to match. As a result, the impedance is best matched in the dual mode.

II. DESIGN AND SIMULATION

The first step in designing a RALA is finding the dipole length $(2D+W_{\rm t})$, illustrated in Fig. 1. Then a proper length of the transmission line needs to be selected so that the antenna radiation pattern is directed towards the right direction and the maximum gain is as high as possible. The list of parameters for the initial simulation is presented in Tab. I.

A. Dipole Length

The effective/guided wavelength ($\lambda_{\rm g}$) of the wave traveling in a microstrip line can be calculated using the following equation,

$$\lambda_{\rm g} = \frac{f_{\rm o}}{\sqrt{\epsilon}} \tag{1}$$

where $f_{\rm o}$ and ϵ are the frequency (Hz) and relative permittivity of the dielectric. $\lambda_{\rm g}$ inside FR4 substrate at 3.5 GHz is 40.8 mm. The length of a half-wavelength ($\lambda_{\rm g}/2$) long dipole would be 20.4 mm.

However, the structure is not completely microstrip. We sweep the D parameter (Fig. 1) from 11.5 mm to 19.5 mm at

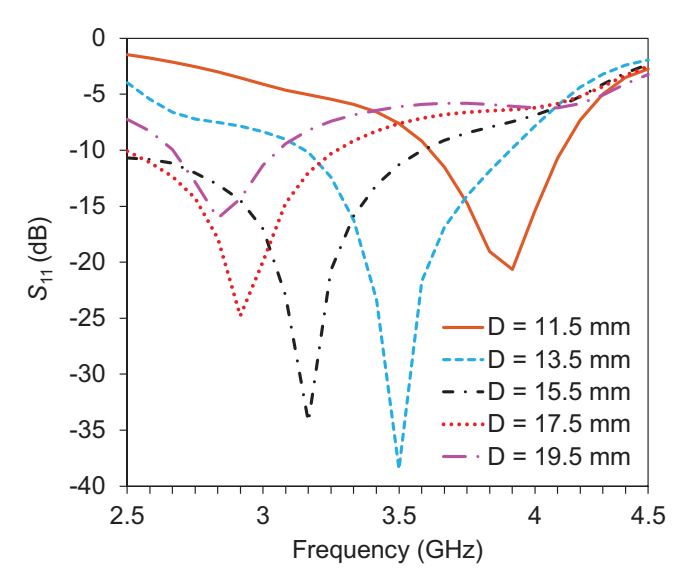


Fig. 2: S_{11} vs. frequency plot for different values of D.

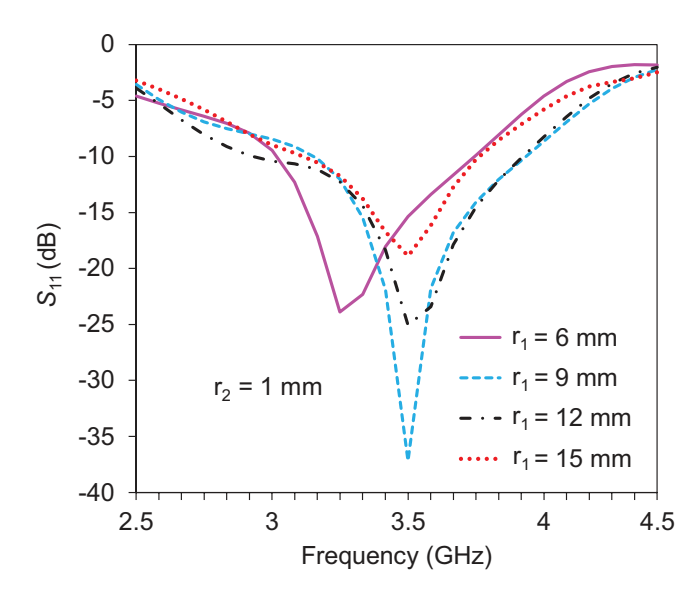


Fig. 3: S_{11} vs. frequency plot for different values of r_2 .

2 mm increments. Fig. 2 shows the reflection coefficient (S_{11}) from 2.5 - 4.5 GHz. The antenna is resonant at 3.5 GHz for D = 13.5 mm.

B. r_1/r_2 Ratio

The radii of the top and bottom layer circles can be used to modify the input impedance of the antenna. In other words, the r_1/r_2 ratio can be used to optimize the antenna bandwidth and resonant frequency. We choose $r_2=1\,$ mm. A smaller value of r_2 would make it difficult to connect the Sub-Miniature version A (SMA) connector whose central pin (1 mm diameter) is connected to the bottom circle (radius r_2). On the other hand, a small value of r_2 allows larger r_1/r_2 ratios. We sweep the r_1 -parameter from 6 mm to 15 mm with a 3 mm step. $Z_{\rm in}$ for

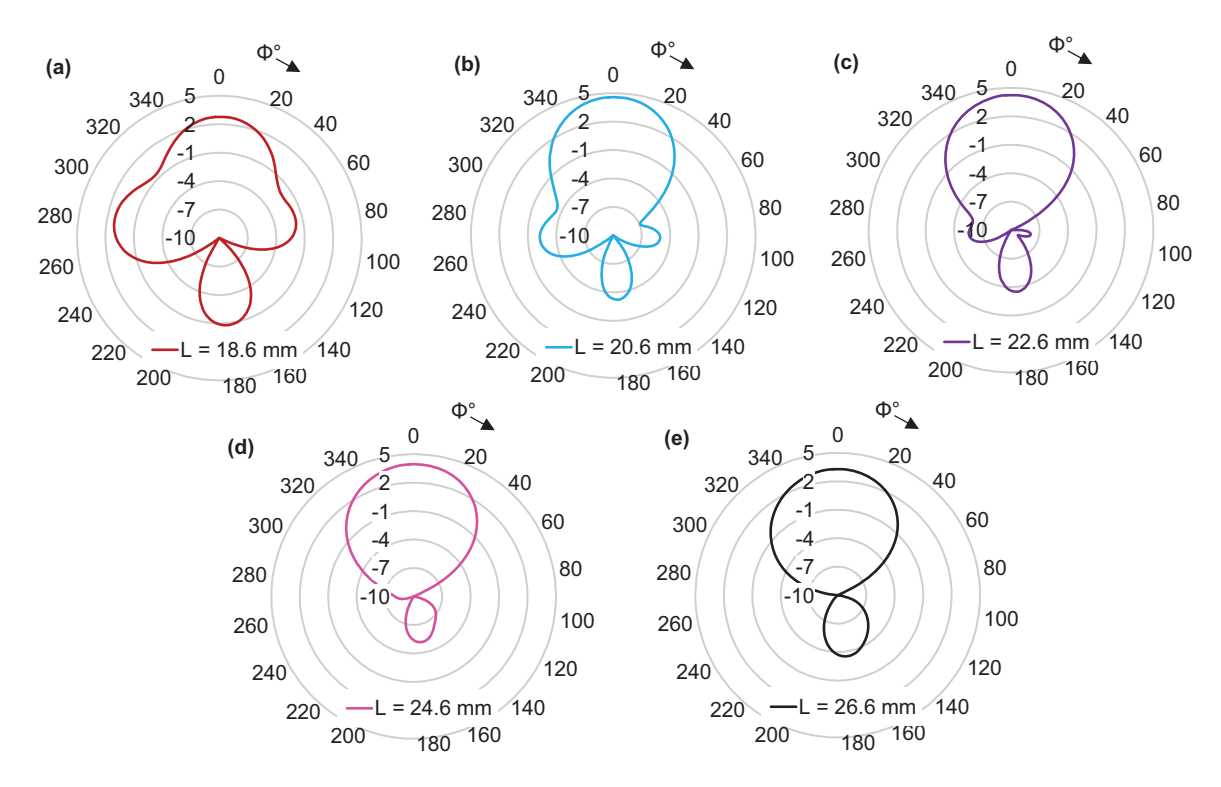


Fig. 4: 2D radiation pattern of the RALA for different values of L - a) 18.6 mm (2.79 dBi maximum gain), b) 20.6 mm (4.58 dBi), c) 22.6 mm (4.26 dBi), d) 24.6 mm (3.94 dBi), e) 26.6 mm (3.29 dBi).

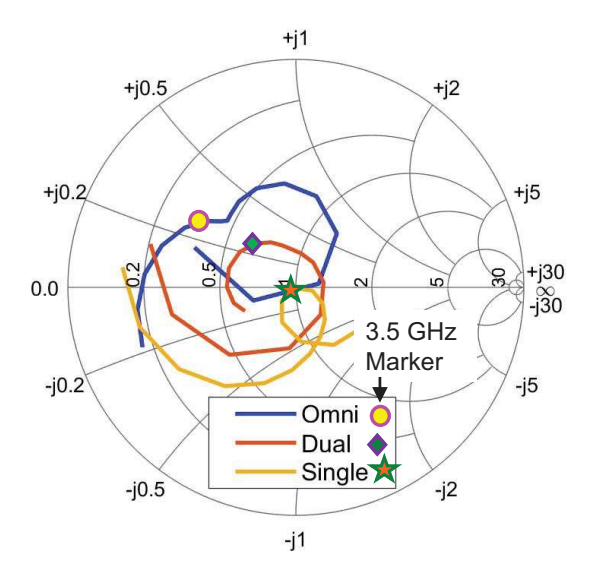


Fig. 5: Smith chart representation of the antenna input impedance in three modes.

these combinations (r_1 = 6, 9, 12, and 15 mm) are 70.6 + j0.2, 50.8 - j1.13, 46.8 + j4.4, and 49.8 + j11.4 Ω , respectively. Fig. 3 shows the reflection coefficient (S_{11}) vs. frequency plot for the r_1 sweep. It is clear that, r_1 = 9 mm gives the best

impedance match and higher quality factor (Q).

C. Radiation Pattern

Dipole antennas have omnidirectional radiation patterns. However, the RALA is a modified planar dipole antenna. The L parameter should be chosen so that L is close to $\lambda_{\rm g}/2$. We run a sweep on the L parameter from 18.6 mm to 26.6 mm with a 2 mm step. Fig. 4 shows the 2D radiation pattern of the single-mode RALA on the $\theta=0^{\circ}({\rm XY-plane})$. The maximum gain is 4.58 dBi for L=20.6 mm (Fig. 4b). However, the resonant frequency moves to 3.6 GHz, and the minimum S_{11} increases to -26.5 dB. On the other hand, for L=22.6 mm, the maximum gain is 4.26 dBi (Fig. 4c) and minimum $S_{11}=-37.2$ dB. In addition, the side lobe level is lower for L=22.6 mm, compared to the 20.6 mm case. As a result, we choose L=22.6 mm.

D. Tri-Mode Antenna Tuning

We designed the antenna in single mode. However, the simulation of the dual and omnidirectional modes show that the input impedance at 3.5 GHz becomes more inductive in the two states. Fig. 5 shows that in the single mode, $Z_{\rm in}$ is at the center of the Smith chart (50 Ω) at 3.5 GHz. The input impedance ($Z_{\rm in}$) values are (50 - j0.3) Ω , (32.8 + j13.6) Ω , and (18.8 + j14.4) Ω in the single, dual, and omnidirectional orientations. It is evident that the antenna input impedance (at 3.5 GHz) becomes increasingly inductive as the number

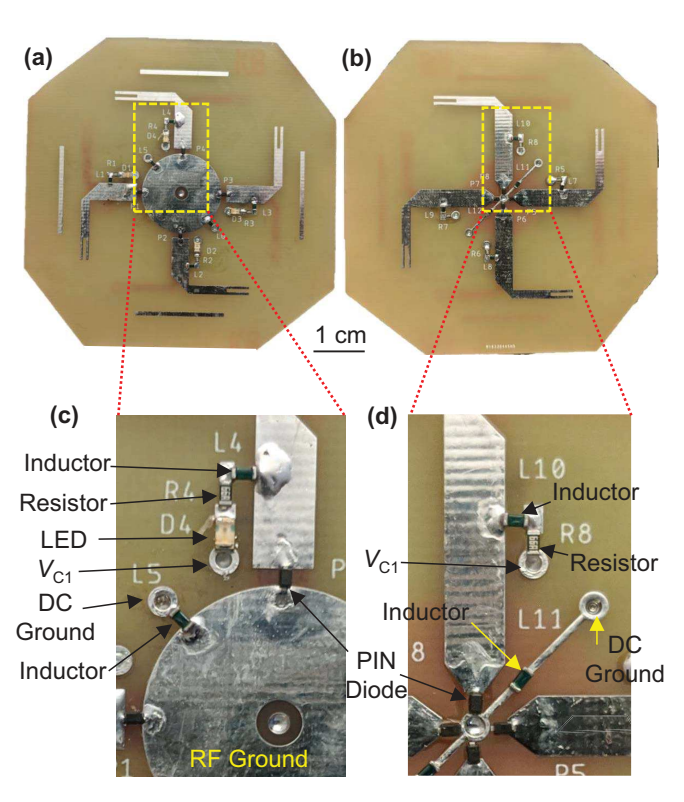


Fig. 6: (a) Top and (b) bottom views of the fabricated RALA, control circuit of a single element on the (c) top and (d) bottom layers.

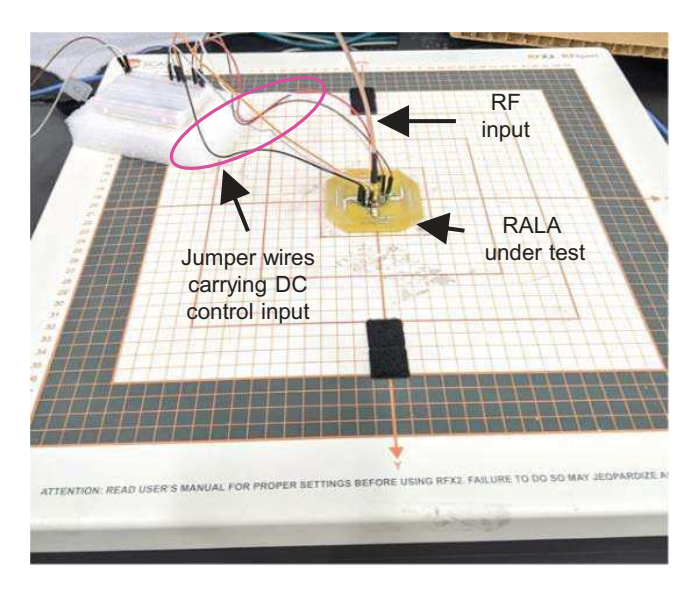


Fig. 7: Radiation pattern test setup on EMScan [15].

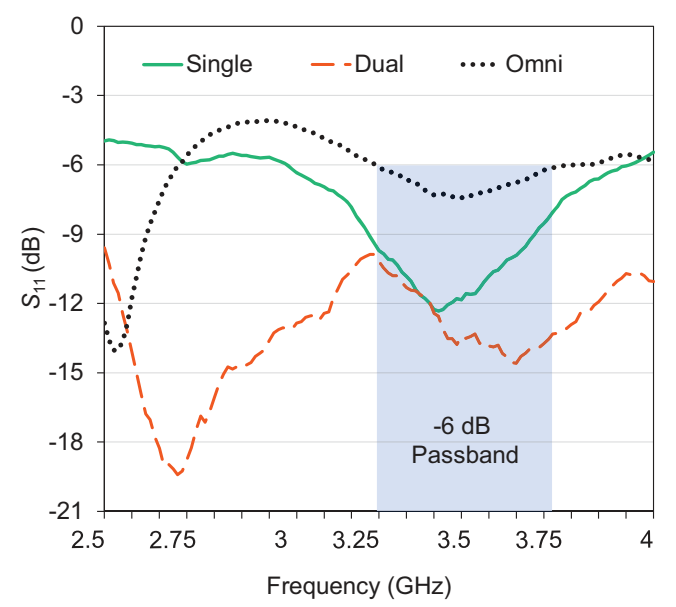


Fig. 8: Measured S_{11} in the single, dual, and omni modes. The -6 dB bandwidth (537 MHz) ranges from 3.24 GHz to 3.78 GHz.

of active antenna elements increases. In addition, the resistive part decreases. All three modes cannot be matched at the same time. There is a trade-off between antenna reconfigurability and impedance match. As a result, the antenna is redesigned so that the antenna is matched at the central (dual) mode. Matching the antenna in the dual mode would make the single mode reactance capacitive and the omni mode inductive. This is achieved by increasing the g-parameter from 0.5 mm to 1 mm

III. FABRICATION, POPULATION, AND MEASUREMENTS

A. Antenna Fabrication

The antenna is fabricated on a double-sided FR4 substrate of 1.6 mm thickness (Fig. 6). There are seven holes drilled into the board. The central hole accommodates the inner conductor (1 mm diameter) of an SMA connector. Two of the holes are used to short the top and bottom DC grounds, and the other four holes accommodate the jumper wires carrying the DC control signals ($V_{\rm C1}$, $V_{\rm C2}$, $V_{\rm C3}$, and $V_{\rm C4}$). The characteristic impedance of the SMA connector is 50 Ω .

B. Control Circuit

The control circuits for the four antenna elements are identical. Fig. 6c and Fig. 6d show the control circuit of a single antenna element on the top and bottom layers, respectively. A jumper wire carrying the $V_{\rm C1}$ is soldered into the control input hole, shorting the top and bottom control pads. On the top layer, a light emitting diode (LED), a resistor (475 Ω , and an inductor (22 nH) is soldered between the control pad and the top transmission line. The LED works as a visual indicator for active antenna elements. The resistor

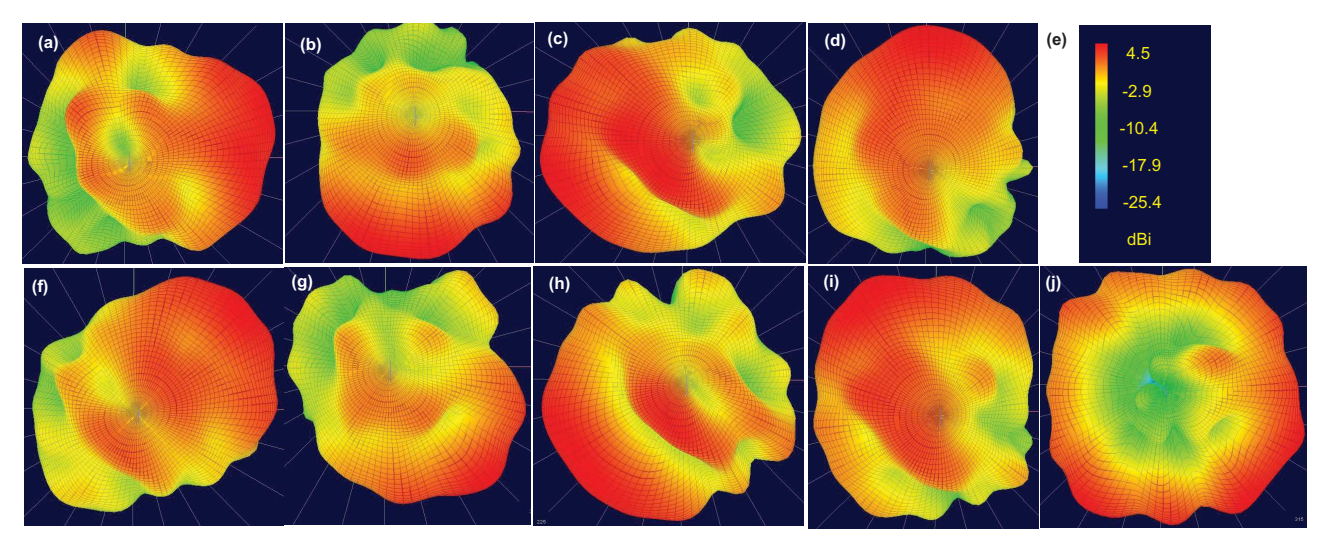


Fig. 9: Radiation patterns measured in EMScan. (a)-(d) single-mode patterns, (e) color-bar showing gain in dBi, (f)-(i) dual-mode patterns, and (j) omni mode radiation pattern.

limits the amount of current, and the inductor works as an radio frequency (RF) choke, blocking RF from entering into the DC control circuit. It is not necessary to block the DC signal from entering the radiating RF components since DC (non-accelerated electrons) cannot generate RF radiation. We ensured that the self-resonant frequency of the inductor is well-above 3.5 GHz. The bottom control circuit (Fig. 6d) is identical to the top layer, except for the LED. The big circle on the top works the RF ground. We place RF choke inductors (22 nH) between the DC ground and the big circle.

C. Antenna Characterization

The reflection coefficient (S_{11}) of the antenna in different modes is measured using a Keysight N5247A network analyzer. DC control signals were generated using a DC source. The directionality of the antenna radiation pattern is measured using an EMScan [15]. The antenna is placed at the center of the EMScan along with the DC control-signal-carrying jumper wires and a coaxial cable running between an RF signal generator and the antenna under test (Fig. 7a). A continuous-wave RF signal at 3.5 GHz was generated using an RF signal generator.

IV. RESULTS AND DISCUSSION

A. Reflection Coefficient, S_{11}

Fig. 8 shows the measured reflection coefficient of the RALA in three different modes. Since the final design was optimized to have better impedance match at the dual mode, the -10 dB passband ranges from 2.5 GHz to 4 GHz. The -10 dB passband for the single mode is 3.3 - 3.7 GHz. The omni mode does not have a -10 dB passband. However, the omni mode has a -6 dB passband ranging from 3.24 GHz to 3.78 GHz. The directionality of the antenna is achieved at the price of limited omni-mode passband. However, the impedance

match in the omni mode can be improved by using a voltagecontrolled matching network dedicated to ensure impedance match at the omni mode.

B. 3D Radiation Pattern

The directionality of the RALA in different modes are confirmed by measuring 3D radiation patterns using an EMScan. Fig. 7b shows the omnidirectional radiation pattern when all four antenna elements were simultaneously activated. Fig. 9 (a-d) depicts the antenna radiation pattern in the single mode, while Fig. 9 (e-h) shows the patterns in the dual mode.

At higher frequencies, the size of the RALA would be smaller. As a result, the space available for the DC control circuit components becomes limited. Moreover, the jumper wires and surface-mount device (SMD) components increase loss in the antenna and reduce the antenna quality factor (Q). The metallic components of the control circuit would also affect the antenna radiation pattern and resonant frequency.

V. Conclusion

In this paper, we presented the techniques and challenges associated with the design of planar reconfigurable Alford Loop antennas. Step-by-step simulations to achieve a RALA centered at 3.5 GHz, that can be used for sub-6 GHz 5G NR applications, are shown. The simulated antenna is fabricated with a 1.6 mm thick double-sided FR4 PCB. In addition, the trade-off between directionality and antenna impedance match is also discussed and analyzed. Reflection coefficient (S_{11}) and 3D radiation patterns are shown for single, dual, and omnidirectional modes.

VI. ACKNOWLEDGMENTS

The author would like to thank Kevin Carbone and Matthew Sigda for their effort in antenna population and performance evaluation. This material is based upon work supported by the National Science Foundation under Grant No. 1730140.

REFERENCES

- B. A. Cetiner, H. Jafarkhani, Jiang-Yuan Qian, Hui Jae Yoo, A. Grau, and F. De Flaviis, "Multifunctional reconfigurable mems integrated antennas for adaptive mimo systems," *IEEE Communications Magazine*, vol. 42, no. 12, pp. 62–70, 2004.
- [2] D. Rodrigo, L. Jofre, and B. A. Cetiner, "Circular beam-steering reconfigurable antenna with liquid metal parasitics," *IEEE Transactions* on Antennas and Propagation, vol. 60, no. 4, pp. 1796–1802, 2012.
- [3] "Skyworks SMP1345 SERIES PIN Diode [Online]," https://www.skyworksinc.com/Products/Diodes/SMP1345-Series, accessed: 2021-03-24
- [4] S. Begashaw, J. Chacko, N. Gulati, D. H. Nguyen, N. Kandasamy, and K. R. Dandekar, "Experimental evaluation of a reconfigurable antenna system for blind interference alignment," in 2016 IEEE 17th Annual Wireless and Microwave Technology Conference (WAMICON), 2016, pp. 1-6
- [5] D. Patron, D. Piazza, and K. Dandekar, "Wideband planar antenna with reconfigurable omnidirectional and directional radiation patterns," *Electronics Letters*, vol. 49, no. 8, pp. 516–518, 2013.
- [6] D. Patron, K. R. Dandekar, and D. Piazza, "A reconfigurable antenna with omnidirectional and directional patterns for mimo systems," in 2013 IEEE Antennas and Propagation Society International Symposium (APSURSI). IEEE, 2013, pp. 204–205.
- [7] D. Patron, A. S. Daryoush, K. R. Dandekar, and D. Piazza, "Design and harmonic balance analysis of a wideband planar antenna having reconfigurable omnidirectional and directional patterns," in WAMICON 2013. IEEE, 2013, pp. 1–5.
- [8] D. Patron and K. R. Dandekar, "Planar reconfigurable antenna with integrated switching control circuitry," in *The 8th European Conference* on Antennas and Propagation (EuCAP 2014). IEEE, 2014, pp. 2737– 2740
- [9] D. Patron, A. S. Daryoush, and K. R. Dandekar, "Optical control of reconfigurable antennas and application to a novel pattern-reconfigurable planar design," *journal of lightwave technology*, vol. 32, no. 20, pp. 3394–3402, 2014.
- [10] G. D. Sworo, D. Patron, K. R. Dandekar, and M. Kam, "Characterization of pattern reconfigurable antenna arrays for mimo systems," in 2015 49th Annual Conference on Information Sciences and Systems (CISS). IEEE, 2015, pp. 1–3.
- [11] D. Patron, D. Piazza, and K. R. Dandekar, "On the use of lumped filters for designing dual-band planar antennas with omnidirectional and directional radiation patterns," in 2015 IEEE 16th Annual Wireless and Microwave Technology Conference (WAMICON). IEEE, 2015, pp. 1–3.
- [12] W. Gao, S. J. Chen, W. Withayachumnankul, and C. Fumeaux, "Horizontally polarized 360° beam-steerable frequency-reconfigurable antenna," *IEEE Transactions on Antennas and Propagation*, vol. 67, no. 8, pp. 5231–5242, 2019.
- [13] N. Gulati and K. R. Dandekar, "Learning state selection for reconfigurable antennas: A multi-armed bandit approach," *IEEE Transactions on Antennas and Propagation*, vol. 62, no. 3, pp. 1027–1038, 2014.
 [14] X. R. Rey, G. Mainland, and K. Dandekar, "Real-time online learning for
- [14] X. R. Rey, G. Mainland, and K. Dandekar, "Real-time online learning for pattern reconfigurable antenna state selection," in 2020 7th NAFOSTED Conference on Information and Computer Science (NICS), 2020, pp. 13–18.
- [15] "EMScan RFxpert [Online]," https://www.emcfastpass.com/test-equipment/shop/near-field-scanners/antenna-characterization-near-field-scanner-emscan-rfxpert-rfx-6/, accessed: 2021-03-24.